Various effects of aliphatic amino acids on the critical current of the MgB_2 superconductor

Grivel, Jean-Claude; Cui, J.; Consuelo-Leal, A.

Published in:
Physica C: Superconductivity and its Applications

Link to article, DOI:
10.1016/j.physc.2020.1353750

Publication date:
2020

Document Version
Peer reviewed version

Physica C 10.1016/j.physc.2020.1353750

Various effects of aliphatic amino acids on the critical current of the MgB_2 superconductor

J.-C. Grivel[1,*], J. Cui[2] and A. Consuelo-Leal[3]

[1]*Department of Energy Conversion and Storage, Technical University of Denmark, Anker Engelunds Vej, DK-2800 Kgs. Lyngby, Denmark*

[2]*College of Materials Science and Engineering, Beijing University of Technology, Beijing 100124, China*

[3]*Instituto de Física de São Carlos, Universidade de São Paulo, CP 369, 13560-970, São Carlos, SP, Brazil*

Abstract

Carbon-doped MgB_2 polycrystalline bulk samples were prepared by reacting mixtures of Mg and B powders, with and without 0.5 wt.% of the amino acids glycine, alanine, valine, leucine or isoleucine. The amount of carbon introduced into the MgB_2 structure depends on the amino acid and is surprisingly higher for glycine, which has the lowest carbon content among the aliphatic amino acids. The critical temperatures of samples doped with all kinds of additives were lower than for the undoped sample. The critical current density was influenced by the additives to different extents, alanine, valine and leucine yielding the best results. The pinning force is also larger for these additives at $T < 30$ K. An analysis of the normalized flux pinning force behavior leads to the conclusion that point pinning is predominant in all samples.

Keywords: MgB_2; doping; carbon; amino acid; glycine; alanine; valine; leucine; isoleucine

Corresponding author: J.-C. Grivel

Email: jean@dtu.dk

Introduction

Polycrystalline superconducting MgB_2 samples are characterized by grain boundaries that do not, or only marginally, suppress the dissipationless critical current density (j_c) [1]. Other interesting properties of this compound from commercial and technological points of view include the low price of the constitutive elements, a reasonably high critical temperature (T_c) of about 39 K and relative ease of synthesis. MgB_2 has already demonstrated its potential for various applications such as high field magnets [2-4], energy storage devices [5,6], high power cables [7], racetrack coils [8], etc. These achievements were realized in the form of demonstration units. In order to be commercially more attractive for market penetration, MgB_2 still requires some improvements in the form of an increase of its $j_c(B)$ performance in the form of long, flexible wires or bulk samples. Indeed, the j_c of pure MgB_2 tends to be significantly lowered when a magnetic field (B) is acting on the material, especially if an operation temperature of 20 K is aimed at. The two strategies that have proven to be most efficient in this view consist in either creating nanoparticle inclusions that act as flux pinning centers [9-14] or doping, preferentially on the B-sites. In the latter case, the most effective doping element for enhancing the j_c of MgB_2 under high magnetic fields is clearly carbon [15-24], whereas other potential B-site dopants such as Al only show limited improvements or even rather adverse effects [25-29]. There exist numerous potential carbon sources for doping MgB_2 during the formation process via reaction between Mg and B powders. Among the most popular organic compounds, malic acid ($C_4H_6O_5$) was shown to result in significant improvements of j_c and of the irreversibility field (B_{irr}) as well as in a reduction of the anisotropy of MgB_2 [30]. Nevertheless, the relatively high oxygen content of malic acid can result in the formation of a large amount of MgO impurities that can potentially impair the performance of superconducting wires and bulk samples. In principle, using carbon sources

characterized by a higher carbon and lower oxygen content (36 wt.% and 60 wt.% respectively for malic acid) might be expected to be more suitable. In this view, an oxygen-free organic precursor would seem an ideal choice. Nevertheless, a comparison of the results reported for C_6H_6 and $C_{12}H_{18}$ [15,31] shows that the effect is highly dependent on the specific compound used as carbon source. The view that carbon atoms substitute for boron in the MgB_2 lattice was challenged by Kim et al. [32], who concluded from their investigations that carbon atoms from malic acid form a thin layer around boron grains prior to MgB_2 formation and remain there, mostly preventing grain growth. On the other hand, boron vacancies that generate stacking faults and lattice distortions, which enhance the upper critical field and the high-field j_c were formed in the lattice. A more nuanced view appears from several reports dealing with graphene coated or generally carbon-encapsulated boron powders, which conclude to partial carbon-boron substitution in MgB_2 and a residual carbon layer at the surface of the MgB_2 grains that generates two-dimensional surface pinning centers and suppresses grain growth [33-37]. In the case of carbon nitride (C_3N_4) coated boron powders, BN nano-inclusions also form and contribute to performance enhancement [38], while for mixing of multiwall carbon nanotubes (MWCNT) to precursor powders, some MWCNTs remain inside the final MgB_2 grains and influence the flux pinning mechanism [39].

Recently, the amino acids glycine and histidine were reported to yield promising results in term of j_c enhancement [40-43]. These compounds contain oxygen, but to a lesser extent than for example malic acid. From these studies, it was clear, like for oxygen-free organic carbon sources, that the two compounds did not result in the same levels of improvements, with glycine being more efficient than histidine. A direct comparison is however not always easy, because some of the reported studies with glycine also involved copper powder additions [42,43]. Copper is among the few elements, like e.g. Ag or Bi, that can decrease the melting point of Mg and thus have an

influence on the reaction process and final microstructure of the MgB_2 polycrystalline samples [44-46]. Nevertheless, samples with only glycine additions exhibit excellent superconducting properties [40]. Since there are many different amino acids, it is worth checking their effect on MgB_2 in a systematic way as they may act in different manners. The purpose of the present work was to compare the influence of 5 closely related amino acids: glycine, alanine, valine, leucine and isoleucine, which are characterized by an increasing carbon to oxygen ratio (Fig. 1 and Table 1). It appears that those with the highest carbon content are not necessarily the most efficient in view of carbon doping.

Experimental details

Magnesium (Alfa Aesar, 99.8 % purity, ≤ 44 μm particle size) and amorphous boron (Aldrich, 95-97 % purity, ≤ 1 μm particle size) powders were first introduced in a polyethylene bottle together with zirconia balls (20 pieces, 80 g in total for 200 g powder) and mixed in a mechanical blender (Bachofen, type T2C). 2 g aliquots of the mixed but yet unreacted powder mixture were mixed with amino acid powders using a similar process. The amino acids consisted of glycine ($C_2H_5NO_2$), alanine ($C_3H_7NO_2$), valine ($C_5H_{11}NO_2$), leucine ($C_6H_{13}NO_2$) and isoleucine ($C_6H_{13}NO_2$), all from Alfa Aesar and with 99 % purity. Mixing was conducted in dry state in 32 ml polyethylene sample holders with 2 zirconia balls. The nominal compositions were: MgB_2 + 0.5 wt.% amino acid. A reference sample without additive was prepared in a similar way, including the second mixing step. In all cases, a slight excess of B (2 at.%) was included to compensate for the impurities (notably some Mg), which are present in the boron powder used in this work [47]. After mixing, the powders were pressed into pellets with 12 mm diameter and 1.5 mm thickness under a pressure of 1.8 kbar. Reaction was performed under static Ar atmosphere at 800°C for 1 h. The heating rate was 100°C/h and the samples were furnace cooled at the end of the treatment.

To reduce the risk of oxidation by the residual O_2 present in the Ar gas (nominally < 0.5 ppm), the pellets were protected by Ti foils acting as oxygen getters.

After reaction, the pellets were cut into several pieces by means of a diamond saw. X-ray diffraction (XRD) patterns were recorded on crushed powders in a Bruker Robot X-ray diffractometer with CuKα radiation (λ = 1.5406 Å). After the acquisition of a first scan, the powders were mixed with silicon powder (Alfa Aesar, 99.999% purity) used as an internal standard and a second scan was run. The lattice parameters were calculated using the UnitCell least square refinement programme [48]. A table-top TM3000 scanning electron microscope (SEM) from HITACHI equipped with a QUANTAX 70 EDS analyser was used to observe the microstructure of polished cross-sections of the reacted samples. Magnetization measurements were conducted in a vibrating sample magnetometer (VSM) from CRYOGENIC Ltd under a magnetic field of 5 mT (zero field conditions) applied parallel to the longest axis of 8.0 x 2.0 x 1.5 mm^3 samples that were cut from the middle of the reacted pellets. The critical temperature (T_c) was determined as the mid-point of the diamagnetic transition and the transition width (ΔT_c) as the temperature interval extending from 10% to 90% of the maximum diamagnetic signal. The critical current density (j_c) was calculated via the Bean model, using magnetisation hysteresis loops, which were recorded on the same samples. These M(H) loops were measured between -5 T and 5 T. However, only the data up to 4 T are used for the calculation of j_c to avoid artefacts originating from the closing of the loops close to the maximum field, which would result in an artificial fast decrease of the $j_c(B)$ dependence close to 5 T.

Results and discussion

Fig.2 contains the XRD patterns of all samples after reaction. MgB_2 is the majority phase, while some MgO is also evidenced in all samples. Traces of unreacted Mg are visible in the samples

prepared form powder mixtures containing the amino acids but the corresponding peaks hardly emerge from the background. The intensity of the MgO peaks is slightly larger when amino acids have been incorporated in the starting powder mixture. This is not surprising considering the presence of oxygen in the additives. Nevertheless, the amount of MgO remains rather low. The lattice parameters of the MgB_2 phase are listed in Table 2. The c-axis lattice parameter is not significantly influenced by the use of amino acids. In contrast, the a-axis lattice parameter is shorter for samples made with amino acid additions, though to various extents. It is also worthwhile noting that the full width at half maximum (FWHM) of the (002) diffraction peak of MgB_2 is only slightly larger in the amino acid added samples, whereas the increase is more significant for the (110) peak. This indicates that the amino acids have induced some disorder especially in the a-b plane of the structure and much less along the c-axis direction. A similar behavior of the lattice parameters is generally observed when MgB_2 is formed in the presence of organic additives [49-55] and this is attributed to the substitution of carbon atoms on boron sites in the lattice. A decrease of the a-axis lattice parameter has also been detected in studies of Mg-deficient MgB_2 [56-58]. In this case, the c-axis lattice parameter is also more or less constant. The fact that Mg peaks are emerging from the background of the XRD patterns when amino acids are used, however, the reported variations of the a-axis lattice parameter in such a case are clearly smaller than those induced by glycine, alanine, valine, leucine and isoleucine. Therefore, the observed change is not primarily due to possible stoichiometry variations, although a minor contribution cannot be ruled out.

A detail of the magnetization measurements around the superconducting transition is plotted in Fig.3. It is obvious that the amino acids resulted in lower T_c values. This observation coupled to the behavior of the lattice parameters suggests that some carbon substitution took place during the reaction process. The amount of C incorporated in the MgB_2 lattice was estimated using the data

published by Lee et al. [59] from both the a-axis lattice parameter contraction (C_{XRD}) and T_c (C_{Tc}). The results are given in Table 2 and compared with the maximum carbon substitution that could be theoretically expected if all the C atoms contained in the additives had actually entered the MgB_2 crystal lattice (C_{nom}). For all amino acids, the C_{XRD} and C_{Tc} values are in relatively good agreement. However, if we compare the experimentally estimated C doping level with the maximum theoretical carbon substitution (C_{nom}), important differences appear. For glycine, all C available in the amino acid seems to enter the MgB_2 lattice, whereas the efficiency of the other four studied amino acids is lower, with a tendency for decreasing uptake as the molar mass of the additive increases. Indeed, in spite of the much larger carbon weight percentage of leucine and isoleucine, the carbon substitution level in the corresponding samples is clearly not higher than for the sample made with glycine additions.

SEM images of the polished cross-sections of all samples are shown in Fig.4(a-f). They are characterized by a relatively dense MgB_2 matrix (light grey) made of small grains. Larger dark grey particles are disseminated in the matrix and are characterized by a lower Mg:B ratio, corresponding mostly to the boron-rich phase MgB_7 according to local EDS measurements. The coherence between the MgB_2 matrix and the higher borides areas is clearly disturbed for the sample doped with alanine, while isoleucine additions also results in elongated cracks running along the boundary between the large boron-rich particles and the matrix. The microstructure of the other samples, including the undoped one, is denser. However, the aspect of the boron-rich areas is strikingly different for the samples with valine and leucine additions, with many MgB_2 inclusions visible as light grey patches embedded inside higher boride, dark grey regions.

The difference in microstructures as well as carbon doping abilities of these 5 amino acids is probably influenced by their behavior under thermal treatment. Several studies relating to their

pyrolysis have been published. Some reported values for the decomposition temperature of glycine, alanine, valine, leucine and isoleucine are listed in Table 1. Although the agreement between different authors is not perfect, all compounds start decomposing in the same temperature range, i.e. below 320°C. However, the decomposition mechanism is very complicated, with a large number of different products that greatly vary depending on the individual amino acids [60-64]. In some cases, the presence of a transient molten phase is still a matter of debate. In the case of the amino acid glutamine for example, decomposition of the amino acid itself takes place in the solid phase, but one of the decomposition products (5-Oxo-L-prolyl-L-glutamine) is liquid at the decomposition temperature [65]. Decomposition kinetics studies show important differences, even just among the aliphatic amino acids in spite of their closely related molecular structures [66]. To complicate the situation even more, leucine was found to sublime upon heating and decompose in the gas phase at a higher temperature so that the mass loss data used for computing decomposition kinetics from thermogravimetric analysis may represent the kinetics of the sublimation process rather than of the decomposition [67]. In view of these considerations, it is very difficult to relate the microstructure of the MgB_2 samples to the thermal behavior of the amino acid additives. There is however one point of importance: the decomposition process of glycine takes place over a much larger temperature interval (extending up to about 575°C) compared to alanine, valine, leucine and isoleucine, which have finished their decomposition process by 350°C [68]. This peculiarity might be the reason behind the more efficient carbon doping ability of glycine, as a large part of the carbon atoms, bond in volatile decomposition products, may have escaped the samples with alanine, valine, leucine or isoleucine additions before the start of the MgB_2 phase. Even more important, a striking result included in the work of Rodante et al. [68] is that the residual mass of alanine, valine, leucine and isoleucine is reduced to zero already at 400°C in thermogravimetric

measurements performed with a heating rate of 10°C/min, whereas the residual mass of glycine still amounted to 35% at 590°C (the maximum reported temperature) with a decreasing mass loss rate. This means that a significant amount of the decomposition products of glycine would still be trapped inside the pellets when the MgB_2 phase starts forming, i.e. around 575°C [69]. A similar observation was recently reported by Huang et al. [70], who still recorded about 20% residual mass at 900°C. In order to better grasp the importance of this observation, a 10 mg sample of glycine powder was heated with a rate of 5°C/min up to 600°C under Ar atmosphere. The residue is shown in Fig.5. A carbonaceous structure has formed, which consists of a very thin, fragile layer surrounding a hole. This configuration suggests that a liquid was formed that was expanded by evolving gas during heating. Under such circumstances, it is not surprising that glycine is a more efficient carbon doping source than alanine, valine, leucine and isoleucine. It might even seem surprising that those latter compounds resulted in carbon substitution at all. However, it cannot be excluded that they formed compounds with Mg or B prior to decomposing during the first stage of the heating process, thus introducing additional complexity to the analysis. A general conclusion that can be drawn from these considerations is that a higher proportion of carbon, although desirable, is not a sufficient condition for classifying an organic compound as an efficient carbon-source for doping in MgB_2. An important characteristic to take into account is the volatility (sublimation, evaporation in case of melting or of liquid decomposition products) of the compounds at temperatures lower than the onset of MgB_2 formation. Indeed, in a porous ceramic, highly volatile compounds can easily escape, thus reducing the amount of carbon available for substitution. In a closed system such as metal-clad wires, the situation is likely to be modified, but the creation of a high gas pressure may also result in serious issues.

The EDS spectrum recorded on a sample with valine additions (Fig.6) reveals the detection of trace amounts of several elements beside Mg and B. Among those, Si is believed to result from the polishing process, because SiC particle suspensions are used during some grinding steps. On the other hand, the presence of S, Cl, Ca and Fe is due to the starting Mg (for Ca) and B powders as previously reported [47,71]. The amino acid powders do not seem to contribute to these impurities as the EDS spectrum of the sample without additions is similar to those of the samples prepared with amino acids. It is important to note that Fe and Ca at least are mostly confined to areas lying outside the MgB_2 matrix. For Ca, elemental analysis allows the identification of the formation of CaB_6 in a few large particle agglomerates as that shown in Fig.7b. In the case of Fe, the smaller particle dimensions prevented a precise determination of the composition Fig.7a. It is however reasonable to assume that Fe reacted with B particles to form Fe_2B like in the case of MgB_2 wires made in Fe tubes by means of the in-situ process (reaction of a Mg and B powder mixture inside the Fe sheath) [72].

The critical current density (j_c) is plotted against the applied magnetic field at 35 K, 30 K, 25 K, 20 K and 15 K in Fig.8. At 35 K, the j_c of the sample doped with isoleucine is clearly lower than that of the sample synthesized without additions. For glycine, alanine, valine and leucine additions, j_c at low field is comparable or even a little higher than that of the reference sample, but a crossover takes place at a field of about 0.2 T, above which the reference sample exhibits higher j_c than all the others. Lowering the temperature improves the performance of the samples made with amino acid additions relative to the reference, pure MgB_2 sample. This is especially clear for alanine, valine and leucine, while the isoleucine added sample has reached a j_c level comparable with that of the reference sample. Surprisingly, the sample made with glycine additions, although having the highest level of carbon substitution, is not among those that perform best in terms of j_c neither

in self field nor under applied magnetic field. This implies that a higher C content is not enough to ensure an optimum performance. Although the j_c improvements seem to continue along the same trend at $T < 20$ K, flux jumps that appear already at 15 K (Fig.8) in some samples (valine and leucine additions) prevent drawing valuable conclusions.

The flux pinning force ($F_p = j_c \cdot B$) calculated for the j_c measurements performed at 15 K, 20 K, 25 K, 30 K and 35 K is shown in Fig.9. At 35 K, $F_p(B)$ is larger in the undoped sample for the whole applied magnetic field range. For 30 K, the $F_p(B)$ of most samples with amino acid additions becomes higher than without additions, but at low fields only. Indeed, from about 1.5 T, all samples except that with isoleucine addition show similar $F_p(B)$ values. However, at 25 K and lower temperature, all samples with additions, with the exception of that with isoleucine exhibit higher pinning forces than the pristine sample at all studied magnetic fields.

In order to obtain some insight into the dominant flux pinning mechanism and possible modifications thereof by the amino acid additives, the normalized pinning force ($f = F_p/F_{pmax}$) , i.e. the pinning force $F_p(B)$ normalized by the maximum value of F_p (= F_{pmax}) has been calculated. The results are plotted versus $b = B/B_{Fpmax}$ i.e. the applied magnetic field B normalized by the field corresponding to F_{pmax}. in Figs.10. The following models were used. Their functional dependence was originally derived for type II superconductors with $\kappa > 1$ in the case of non-magnetic pinning centers and correspond to surface pinning (1), normal point pinning (2) and $\Delta\kappa$ pinning (3) [73,74]:

$$f(b) = \frac{25}{16}\sqrt{b}\left(1-\frac{b}{5}\right)^2 \qquad (1)$$

$$f(b) = \frac{9}{4}b\left(1-\frac{b}{3}\right)^2 \qquad (2)$$

$$f(b) = 3b^2\left(1 - \frac{2b}{3}\right) \quad (3)$$

For equation (1), the pinning centers have two dimensions larger than the inter-flux-line spacing, while in equation (2) point pins with dimensions less than the inter-flux-line spacing in all directions are considered. For equation (3), the pinning centers manifest themselves as local differences in critical temperature, critical field or Ginsburg-Landau parameter (κ).

In the present case, for $b \leq 1$, all *f(b)* curves coincide and hence indicate a similar flux pinning behavior notwithstanding of initial composition or measurement temperature. The data fall in between the calculated curves based on the point pinning and $\Delta\kappa$ pinning models. It can thereby be inferred that these two types of pinning both contribute to the observed *f(b)* behaviour. Nevertheless, the largest contribution is probably originating from point pinning, because the experimental data are closer to the corresponding model. For $f(b) > 1$, up to approximately $b = 2$, all samples seem to follow more closely the point pinning mechanism model. At $b > 2$, an upwards deviation is observed for all samples at 35 K, 30 K and 25 K, giving the impression of a shift towards the surface pinning behavior. An upwards shift of the *f(b)* curves at $b > 1$ has already been observed several times in relation to carbon doping in MgB_2 [22,75-79]. An upwards shift of the $f(b)$ curves may be an indication that the flux pinning centers responsible for point pinning are not strong enough to withstand the increasingly strong Lorentz acting at high magnetic fields. In such a case, the $f(b)$ data tend to leave the point pinning simulation and move towards the surface pinning mechanism that still acts at higher field, becoming the dominant contribution. This effect is reinforced in the samples made with amino acid additions. The increase of the FWHM of the XRD peaks of carbon-doped MgB_2 reflects an increase of microstrain and should not result in a weakening of the overall point pinning. Instead, the enhanced shift towards surface pinning

behavior at high field could be a result of a reinforced surface pinning strength that might be due to some carbon deposition on MgB_2 grain surfaces [33-37]. From these measurements, it is however difficult to conclude whether this deviation really reflects a change in the flux pinning mechanism. For b > 2, the applied field approaches the irreversibility field and the induced superconducting current may not flow around the whole circumference of the sample anymore. However, for the critical current density calculations with the Bean model, the sample size was assumed to be the length scale of the induced current for all measurement conditions and $j_c(B)$, $F_p(B)$ as well as $f(b)$ may not be accurately estimated at the highest temperatures and fields. At 20 K and 15 K, the downwards deviation of the $f(b)$ curves is an artefact due to the closing of the $M(H)$ loops used for the VSM measurements and is not related to an intrinsic physical effect.

The present measurements confirm the beneficial role of glycine additions on the $j_c(B)$ performance of MgB_2 [40] and show that such an effect can also be achieved by use of other amino acids. It is remarkable that, although glycine appears to be the most efficient carbon doping source among the 5 amino acids tested in this study, it does not result in the largest improvements. Since for alanine, valine and leucine additions, larger $j_c(B)$ and $F_p(B)$ values can be obtained for lower actual carbon doping levels than for glycine, it is clear that other effects than only carbon doping are playing a role in the behavior of MgB_2 samples. A better understanding of the intricate interrelationship between organic acid additions and performance requires more systematic studies to determine the optimum synthesis conditions. An encouraging result is that most additives result in an improvement of j_c in self-field, on top of the usual high-field enhancement due to carbon doping in general, which is not always the case [80-82]. These types of additives are therefore promising for superconducting wires. A direct application of these new results to the manufacture of MgB_2 wires will nevertheless also require additional studies since the metal sheath surrounding

the MgB_2 core will certainly have an influence on the kinetics of decomposition and release of gas species resulting from the decomposition of the organic additives.

Conclusion

The efficiency of the amino acids Glycine, alanine, valine, leucine and isoleucine as carbon sources for introducing C in the lattice of the MgB_2 superconductor is strongly dependent on the individual amino acid, with a more efficient transfer of the carbon atoms from glycine to MgB_2 and an apparently decreasing carbon uptake for increasing aliphatic chain length. In spite of this, the highest critical current density and pinning force are obtained for valine, alanine and leucine additions. Since the flux pinning mechanism is the same for all doped samples, it can be concluded that the differences in critical current densities are linked to differences in the microstructure of the samples, which may result from the various decomposition paths of the amino acids. In view of potential applications, it worth noting that most of these amino acid additions result in improvements not only under high applied magnetic fields, but under self-field as well. Other amino acids such as cysteine and methionine contain sulfur, while others (e.g. arginine and glutamine) contain more than one NH_2 group. In both cases, different effects might be expected, which will be worth exploring.

Acknowledgements

Mr. Henrik Paulsen is gratefully acknowledged for preparing the polished cross-sections of the samples for SEM investigations.

Figure captions

Figure 1: Structures of the 5 amino acids used in the present study. They only differ by the length and configuration of the hydrocarbon chain bound to the glycine unit.

Figure 2: XRD patterns of the powdered samples after heat treatment at 800 ^{o}C. The (*hkl*) indices refer to peaks from MgB_2. The expected position and relative intensities of pure MgB_2 according to reference card [74-982] are shown at the bottom of the figure for comparison.

Figure 3: Details of the magnetic susceptibility measurements (VSM) showing the transition between the normal and superconducting states in samples with and without amino acid additions.

Figure 4: SEM images (backscattering mode) of polished cross-sections of samples with amino-acid additions after reaction at 800 ^{o}C: (a) no additive, (b) glycine, (c) alanine, (d) valine, (e) leucine and (f) isoleucine. The same magnification was used for all images.

Figure 5: Solid residue of a 10 mg glycine powder sample heated under flowing Ar at 5 ^{o}C/min up to 600^{o}C in an Al_2O_3 crucible with 5 mm diameter.

Figure 6: Elemental analysis (EDS) of the area corresponding to Fig. ?(f), i.e. 0.5 wt.% addition of valine. The plot shows a detail of the spectrum evidencing the presence of trace amounts of Fe, Ca, Cl, S and Si.

Figure 7: Superposition of the EDS maps for Ca and Fe on two corresponding SEM images (sample with valine addition).

Figure 8: Critical current density ($j_{c)}$ at 35 K, 30 K, 25 K, 20 K and 15 K, calculated from magnetization measurements.

Figure 9: Pinning force (F_p) at 35 K, 30 K, 25 K, 20 K and 15 K versus applied magnetic field (B) for all samples.

Figure 10: Normalized pinning force $f = F_p/F_{pmax}$ at 35 K, 30 K, 25 K, 20 K and 15 K versus the normalized magnetic field $b = B/B_{Fpmax}$. The data for the pure sample and those with different amino acid additives are compared to theoretical predictions of three flux pinning mechanism models: surface pinning (S), point pinning (P) and $\Delta\kappa$ pinning (K).

Table captions

Table 1: Composition, relative carbon content and reported melting/decomposition temperature of the amino acids used in the present study.

Table 2: Cell parameters (*a* and *c*-axis) of the MgB_2 compound formed in the samples with all studied additives. Their critical temperature (T_c) and associated transition width (ΔT_c) (determined as the temperature interval between 10% and 90% of the maximum diamagnetic signal). The full width at half maximum (FWHM) of the MgB_2 (002) and (110) X-ray diffraction peaks. The carbon content was estimated from the variation of the *a*-axis cell parameter (C_{XRD}) and the decrease of the T_c values (C_{Tc}) relative to the sample without additions. The theoretically maximum possible carbon doping level (C_{nom}) in MgB_2 was calculated assuming full substitution of the nominally available carbon included in the additives.

References

[1] D.C. Larbalestier, L.D. Cooley, M.O. Rikel, A.A. Polyanskii, J. Jiang, S. Patnaik, X.Y. Cai, D.M. Feldmann, A. Gurevich, A.A. Squitieri, M.T. Naus, C.B. Eom, E.E. Hellstrom, R.J. Cava, K.A. Regan, N. Rogado, M.A. Hayward, T. He, J.S. Slusky, P. Khalifah, K. Inumaru and M. Haas, Strongly linked current flow in polycrystalline forms of the superconductor MgB_2, Nature 410 (2001) 186 - 189

[2] Y.G. Kim, J.M. Kim, K.H. Kim, H.S. Noh, H.S. Kim, D.Y. Hwang and H.G. Lee, Enhancement of charging and discharging rates for partially insulated MgB_2 magnets composed of Cr-coated MgB_2 superconducting wires, Results in Physics 15 (2019) 102754

[3] D.A. Abin, N.A. Mineev, M.A. Osipov, S.V. Pokrovskii and I.A. Rudnev, Dry cryomagnetic system with MgB_2 coil, J, Phys. Conf. Ser. 941 (2017) 012056

[4] J. Liu, H. Ma, L. Huang and P. Ju, Research on an axial Maglev device with primary superconductive coils for a 1000 MW hydraulic generator set, IEEE Trans. Appl. Supercond. 27 (2017) 5000106

[5] S. Mizuno, T. Yagai, T. Okubo, S. Mizuochi, M. Kamibayashi, M. Jinbo, T. Takao, Y. Makida, T. Shintomi, N. Hirano, T. Komagome, K. Tsukada, Y. Onji, Y. Arai, M. Tomita, D. Miyagi, M. Tsuda and T. Hamajima, Feasibility study of MgB_2 cable for pancake coil of energy storage device, IEEE Trans. Appl. Supercond. 28 (2018) 4602505

[6] A. Morandi, A. Anemona, G. Angeli, M. Breschi, A. Della Corte, C. Ferdeghini, C. Gandolfi, G. Grandi, G. Grasso, L. Martini, U. Melaccio, D. Nardelli, P.L. Ribani, S. Siri, M. Troppeano, S. Turtù and M. Vignolo, The DRYSMES4GRID project: Development of a 500 kJ/200 kW cryogen-free cooled SMES demonstrator based on MgB_2, IEEE Trans. Appl. Supercond. 28 (2018) 5700205

[7] K. Konstantopoulou, A. Ballarino, A. Gharib, A. Stimac, M. Garcia Gonzalez, A.T. Perez Fontenla and M. Sugano, Electro-mechanical characterization of MgB_2 wires for the superconducting link project at CERN, Supercond. Sci. Technol. 29 (2016) 084005

[8] F. Karaboga, H. Yetis, M. Akdogan, D. Gajda and I. Belenli, Design, fabrication, and testing of MgB_2/Fe racetrack coil, IEEE Trans. Appl. Supercond. 28 (2018) 6200805

[9] J. Wang, Y. Bugoslavsky, A. Berenov, L. Cowey, A.D. Caplin, L.F. Cohen, L.D. Cooley, X. Song and D.C. Larbalestier, High critical current density and improved irreversibility field in bulk MgB_2 made by a scalable, nanoparticle addition route, Appl. Phys. Lett. 81 (2002) 2026 – 2028

[10] G.J. Xu, J.-C. Grivel, A.B. Abrahamsen and N.H. Andersen, Enhancement of the irreversibility field in bulk MgB_2 by TiO_2 nanoparticle addition, Physica C 406 (2004) 95 - 99

[11] E. Babic, N. Novosel, D. Pajic, S. Galic, K. Zadro and D. Drobac, Magnetic nanoparticles in MgB_2: vortex pinning, pair breaking and connectivity, J. Magn. Magn. Mater. 400 (2016) 88 – 92

[12] D. Goto, T. Machi, Y. Zhao, N. Koshizuka, M. Murakami and S. Arai, Improvement of critical current density in MgB_2 by Ti, Zr and Hf doping, Physica C 392 (2003) 272 - 275

[13] N. Novosel, S. Galic, D. Pajic, K. Zadro and E. Babic, Enhancing superconducting properties of MgB_2 by addition of magnetic particles, J. Supercond. Nov. Magn. 28 (2015) 425 – 430

[14] L.B.S. Da Silva, A. Serquis, E.E. Hellstrom and D. Rodrigues Jr., Artificial pinning centers in MgB_2 superconducting bulks, Supercond. Sci. Technol. 33 (2020) 045013

[15] M.G. Babaoglu, S. Safran, Ö.Civek, H. Ail, E. Ertekin, Md. Shahriar, A. Hossein, E. Yanmaz and A. Gencer, Microstructural and superconducting properties of C_6H_6 added bulk MgB_2 superconductor, J. Magn. Magn. Mater. 324 (2012) 3455 – 3459

[16] S.X. Dou, O. Shcherbakova, W.K. Yeoh, J.H. Kim, S. Soltanian, X.L. Wang, C. Senatore, R. Flükiger, M. Dhalle, O. Husnjak and E. Babic, Mechanism of enhancement in electromagnetic properties of MgB_2 by nano SiC doping, Phys. Rev. Lett. 98 (2007) 097002

[17] S. Soltanian, J. Horvat, X.L. Wang, P. Munroe and S.X. Dou, Effect of nano-carbon particle doping on the flux pinning properties of MgB_2 superconductor, Physica C 390 (2003) 185 – 190

[18] C.H. Cheng, H. Zhang, Y. Zhao, Y. Feng, X.F. Rui, P. Munroe, H.M. Zeng, N. Koshizuka and M. Murakami, Doping effect of nano-diamond on superconductivity and flux pinning in MgB_2, Supercond. Sci. Technol. 16 (2003) 1182 – 1186

[19] W. Haessler, P. Kováč, M. Eisterer, A.B. Abrahamsen, M. Hermann, C. Rodig, K. Nenkov, B. Holzapfel, T. Melisek, M. Kulich, M. v Zimmermann, J. Bernarcik and J.-C. Grivel, Anisotropy of the critical current in MgB_2 tapes made of high energy milled precursor powder, Supercond. Sci. Technol. 23 (2010) 065011

[20] J.M. Parakkandy, M. Shahabuddin, M. Shahabuddin Shah, N.S. Alzayed, S.A.S. Qaid, N.M. Ramay and M.A. Shar, Effect of glucose doping on the MgB_2 superconductors using cheap crystalline boron, Physica C 519 (2015) 137 – 141

[21] L.B.S. Da Silva, A.A. Vianna, A.L.R. Manesco, E.E. Hellstrom and D. Rodrigues Jr., The influence of stearic acid addition on the superconducting properties of MgB_2, IEEE Trans. Appl. Supercond. 26 (2016) 7100204

[22] J.H. Kim, S.X. Dou, M.S.A. Hossain, X. Xu, J.L. Wang, D.Q. Shi, T. Nakane and H. Kumakura, Systematic study of a MgB_2 + $C_4H_6O_5$ superconductor prepared by the chemical solution route, Supercond. Sci. Technol. 20 (2007) 715 - 719

[23] Z. Gao, Y. Ma, X. Zhang, D. Wang, Z. Yu, K. Watanabe, H. Yang and H. Wen, Strongly enhanced critical current density in MgB_2/Fe tapes by stearic acid and stearate doping, Supercond. Sci. Technol. 20 (2007) 485 – 489

[24] C. Li, H. Suo, M. Liu, L. Ma, Y. Wang, M. Tian, B. Wan, J. Cui and Y. Ji, Effect of malonic acid and of different doping methods on the superconducting properties of MgB_2 superconductors, Physica C 555 (2018) 60 - 65

[25] B. Kang, M.-S. Park, H.-S. Lee, M.-H. Jung and S.-I. Lee, Comparison between Al and C substitutions in the upper critical field of MgB_2 single crystals, J. Kor. Phys. Soc. 58 (2011) 498 - 502

[26] J.Y. Xiang, D.N. Zheng, J.Q. Li, S.L Li, H.H Wen and Z.X.Zhao, Effects of Al doping on the superconducting and structural properties of MgB_2, Physica C 386 (2003) 611-615

[27] G.J. Xu, J.-C. Grivel, A.B Abrahamsen, X.P. Chen and N.H. Andersen, Structure and superconductivity of double-doped $Mg_{1-x}(Al_{0.5}Li_{0.5})_xB_2$, Physica C 399 (2003) 8-14

[28] G.J. Xu, J.-C. Grivel, A.B Abrahamsen, X.P. Chen and N.H. Andersen, Superconducting properties of Zn and Al double-doped $Mg_{1-x}(Zn_{0.5}Al_{0.5})_xB_2$, Physica C 403(2004) 113-118

[29] A.Yu. Potanin, D.Yu. Kovalev, E.A. Levashov, P.A. Loginov, E.I. Patsera, N.V. Shvyndina, K.S. Pervakov, V.A. Vlasenko and S.Yu. Gavrilkin, The features of combustion synthesis of aluminium and carbon doped magnesium diboride, Physica C 541 (2017) 1 – 9

[30] S.A.A. Hossain, M. Mustapic, D. Gajda, C. Senatore, D. Patel, Y. Yamauchi, M. Shahbazi and R. Flükiger, Significant reduction of critical current anisotropy in malic acid treated MgB_2 tapes, J. Magn. Magn. Mater. 497 (2020) 166046

[31] H. Ağıl, E. Aksu, S. Aktürk and A. Gencer, The effects of structural, thermal, and magnetic properties of hexylbenzene-doped MgB_2 superconductor, J. Supercond. Nov. Magn. 30 (2017) 1727 – 1736

[32] J.H. Kim, S. Oh, Y.-U. Heo, S. Hata, H. Kumakura, A. Matsumoto, M. Mitsuhara, S. Choi, Y. Shimada, M. Maeda, J.L. MacManus-Driscoll and S.X. Dou, Microscopic role of carbon on MgB_2 wire for critical current density comparable to NbTi, NPG Asia Materials 4 (2012) 1-7

[33] W. Li, J. Kang, Y. Liu, M. Zhu, Y. Li, J. Qu, R. Zheng, J. Xu and B. Liu, Extrinsic two-dimensional flux pinning centers in MgB_2 superconductors induced by graphene-coated boron, ASC Applied Materials & Interfaces 11 (2019) 10818 – 10828

[34] H. Liu, J. Li, M. Sun, J. Qu, R. Zheng, J.M. Cairney, M. Zhu, Y. Li and W. Li, Carbon-coating layers on boron generated high critical current density in MgB_2 superconductor, ASC Applied Materials & Interfaces 12 (2020) 8563 – 8572

[35] W.K. Yeoh, X.Y. Cui, B. Gault, K.S.B. De Silva, X. Xu, H.W. Liu, H.-W. Yen, D. Wong, P. Bao, D.J. Larson, I. Martin, W.X. Li, R.K. Zheng, X.L. Wang, S.X. Dou and S.P. Ringer, Nanoscale 5 (2014) 6166 – 6172

[36] J.H. Kim, S. Oh, H. Kumakura, A. Matsumoto, Y.-U. Heo, K.-S. Song, Y.-M. Kang, M. Maeda, M. Rindfleisch, M. Tomsic, S. Choi and S.X. Dou, Tailored materials for high-performance MgB_2 wire, Adv. Mater. 23 (2011) 4942 – 4946

[37] D. Kumar, M. Muralidhar, M. Higuchi, M.S. Ramachandra Rao and M. Murakami, Raman spectroscopy o carbon doped MgB_2 prepared using carbon encapsulated boron as precursor, J. Alloys & Compounds 723 (2017) 751 - 756

[38] W. Li, J. Li, Y. Liu, J. Qu, B. Liu, M. Zhu, Y. Li, Z. Huang and R. Zheng, Artificial 2D flux pinning centers in MgB_2 induced by graphitic-carbon nitride coated on boron for superconductor applications, ASC Applied Nano Mater. 2 (2019) 5399 – 5408

[39] I. Ahmad, J.S. Hansdah, S.N. Sarangi and P.M. Sarun, Enhanced magnetic field dependent critical current density of MWCNT doped magnesium diboride superconductor, J. Alloys & Compounds 834 (2020) 155033

[40] Q. Cai, Y. Liu, Q. Guo and Z. Ma, Scattering effect of the well-ordered MgB_4 impurity phase in two-step sintered polycrystalline MgB_2 with glycine addition, Appl. Phys. A 123 (2017) 229

[41] Q. Cai, Y. Liu, Z. Ma and L. Yu, Effect of MgO evolution on the critical current density in bulk MgB_2 containing histidine, Physica C 496 (2014) 53 – 57

[42] Q. Cai, Y. Liu, Z. Ma, L. Yu, J. Xiong and H. Li, Pinning behavior of glycine-doped MgB_2 bulks with excellent critical current density by Cu-activated low-temperature sintering, J. Alloys Compounds 585 (2014) 78 – 84

[43] Q. Cai, Y. Liu, Z. Ma, L. Yu and H. Li, Enhancement of synthesis efficiency and critical current density in glycine-doped MgB_2 bulks by two-step sintering, J. Mater. Sci. Mater. Electron. 28 (2017) 5645 – 5651

[44] J.-C. Grivel, A. Abrahamsen and J. Bednarčik, Effects of Cu or Ag additions on the kinetics of MgB_2 phase formation in Fe-sheathed wires, Supercond. Sci. Technol. 21 (2008) 035006

[45] J.-C. Grivel, N.H. Andersen, P.G.A.P. Pallewatta, Y. Zhao and M.v. Zimmermann, Influence of Bi, Se and Te additions on the formation temperature of MgB_2, Supercond. Sci. Technol. 25 (2012) 015010

[46] Y. Hishinuma, A. Kikuchi, K. Matsuda, K. Nishimura, Y. Kubota, S. Hata, S. Yamada and T. Takeuchi, Microstructure and superconducting properties of Cu addition MgB_2 multifilamentary wires using boron isotope powder as the boron source material, Physics Procedia 36 (2012) 1486-1491

[47] J.C. Grivel, A. Alexiou, K. Rubešová, X. Tang, N.H. Andersen, M. von Zimmermann and A. Watenphul, Preparation and characterization of $Mg_{1-x}B_2$ bulk samples and Cu/Nb sheathed wires with low grade amorphous boron powder, J. Supercond. Nov. Magn. 27 (2014) 497-504

[48] T.J.B. Holland and S.A.T. Redfern, Unit cell refinement from powder diffraction data: The use of regression diagnostics, Mineral. Mag., 61 (1997) 65-77.

[49] N. Ohja, V.K. Malik, R. Singla, C. Bernhard and G.D. Varma, The effect of citric acid and oxalic acid doping on the superconducting properties of MgB_2, Supercond. Sci. Technol. 22 (2009) 125014

[50] J.M. Parakkandy, M. Shahabuddin, M. Shahabuddin Shah, N.S. Alzayed and N.A. Madhar, Effect of ball milling time on critical current density of glucose-doped MgB_2 superconductors, 28 (2015) 475 - 479

[51] M.S.A. Hossain, J.H. Kim, X.L. Wang, X. Xu, G. Peleckis and S.X. Dou, Enhancement of flux pinning in a MgB_2 superconductor doped with tartaric acid, Supercond. Sci. Technol. 20 (2007) 112 - 116

[52] M.S.A. Hossain, J.H. Kim, X. Xu, X.L. Wang, M. Rindfleisch, M. Tomic, M.D. Sumption, E.W. Collings and S.X. Dou, Significant enhancement of H_{c2} and H_{irr} in $MgB_2 + C_4H_6O_5$ bulks at low sintering temperature of 600ºC, Supercond. Sci. Technol. 20 (2007) L51 – L54

[53] A. Vajpayee, V.P.S. Awana, G.L. Bhalla, P.A. Bhobe, A.K. Nigan and H. Kishan, Superconducting properties of adipic-acid-doped bulk MgB_2 superconductor, Supercond. Sci Technol. 22 (2009) 015016

[54] J.H. Kim, S. Zhou, M.S.A. Hossain, A.V. Pan and S.X. Dou, Carbohydrate doping to enhance electromagnetic properties of MgB_2 superconductors, Appl. Phys. Lett. 89 (2006) 142505

[55] J. Li, H. Liu, C. Cai, S. Dou and W. Li, Research progress of electromagnetic properties of MgB_2 induced by carbon-containing materials addition and process techniques, Acta Metallurgica Sinica (English Letters) 33 (2020) 471 - 489

[56] C.H. Jiang and H. Kumakura, Stoichiometry dependence of the critical current density in pure and nano-SiC doped MgB_2/Fe tapes, Physica C 451, (2007) 71 - 76

[57] S.K. Chen, A. Serquis, G. Serrano, K.A. Yates, M.G. Blamire, D. Guthrie, J. Cooper, H. Wang, S. Margadonna and J.L. MacManus-Driscoll, Structural and superconducting property variations with nominal Mg non-stoichiometry in Mg_xB_2 and its enhancement of upper critical field, Advanced Functional Materials 18 (2008) 113 - 120

[58] G.J. Xu, R. Pinholt, J. Bilde-Sørensen, J.C. Grivel, A.B. Abrahamsen and N.H. Andersen, Effect of starting composition and annealing temperature on irreversibility field and critical current density in Mg_xB_2, Physica C 434 (2006) 67 – 70

[59] S. Lee, M. Takahiko, A. Yamamoto, H. Uchiyama and S. Tajima, Carbon-substituted MgB_2 single crystals, Physica C 397 (2003) 7 – 13

[60] Y.C. Lien and W.W. Nawar, Thermal decomposition of some amino acids, J. Food Sci. 39 (1974) 911 – 913

[61] P.G. Simmonds, E.E. Medley, M.A. Ratcliff and G.P. Shulman, Thermal decomposition of aliphatic monoamino-monocarboxylic acids, Anal. Chem. 44 (1972) 2060 – 2066

[62] M.A. Ratcliff, Jr., E.E. Medley and P.G. Simmonds, Pyrolysis of amino acids. Mechanistic considerations, J. Org. Chem. 39 (194) 1481 – 1490

[63] G. Chiavari and G.C. Galletti, Pyrolysis-gas chromatography/mass spectrometry of amino acids, J. Anal. Appl. Pyrol. 24 (1992) 123 – 137

[64] V.A. Basiuk, Pyrolysis of valine and leucine at 500°C: identification of less-volatile products using gas chromatography-Fourier transform infrared spectroscopy-mass spectroscopy, J. Anal. Appl. Pyrol. 47 (1998) 127 - 143

[65] I.M. Weiss, C. Muth, R. Drumm and H.O.K. Kirchner, Thermal decomposition of the amino acids glycine, cysteine, aspartic acid, asparagine, glutamic acid, glutamine, arginine and histidine, BMC Biophysics 11 (2018) 2

[66] W. Tang, C. Wang and D. Chen, An investigation of the pyrolysis kinetics of some aliphatic amino acids, J. Anal. Appl. Pyrolysis 75 (2006) 49 - 53

[67] J. Li, Z. Wang, X. Yang, L. Hu, Y. Liu and C. Wang, Decomposing or subliming? An investigation of thermal behavior of L-leucine, Thermochim. Acta 447 (2006) 147 – 153

[68] F. Rodante, G. Marrosu and G. Catalani, Thermal analysis of some α-amino acids with similar structures, Thermochim. Acta 194 (1992) 197 – 213

[69] J.-C. Grivel, R. Pinholt, N.H. Andersen, P. Kovač, I. Hušek and J. Homeyer, In situ investigations of phase transformations in Fe-sheathed MgB_2 wires, Supercond. Sci. Technol. 19 (2006) 96 - 101

[70] M. Huang, S. Lv and C. Zhou, Thermal decomposition of glycine in nitrogen atmosphere, Thermochim. Acta 552 (2013) 60 - 64

[71] J.-C. Grivel and K. Rubešová, Increase of the critical current density of MgB_2 superconducting bulk samples by means of methylene blue dye additions, Physica C 565 (2019) UNSP 1353506

[72] J.-C. Grivel, N.H. Andersen, R. Pinholt, P. Kovač, I. Hušek, W. Hassler, M. Hermann, O. Perner, C. Rodig and J. Homeyer, In-situ studies of Fe_2B phase formation in MgB_2 wires and tapes by means of high-energy x-ray diffraction, J. Phys. Conf. Ser. 43 (2006) 123 - 126

[73] T. Goto, K. Inagaki and K. Watanabe, Critical current density in filamentary (Nd, Sm, Eu, Gd) – Ba – Cu – O superconductors prepared by a solution spinning method, Physica C 330 (2000) 51 – 57

[74] D. Dew-Hughes, Flux pinning mechanisms in type II superconductors, Phil. Mag. 30 (1974) 293 - 305

[75] J.-C. Grivel, Critical current density improvements in MgB_2 superconducting bulk samples by K_2CO_3 additions, Physica C 550 (2018) 1 – 6

[76] S. Ueda, J.-I. Shimoyama, A. Yamamoto, S. Horii and K. Kishio, Enhanced critical current properties observed in Na_2CO_3-doped MgB_2, Supercond. Sci. Technol. 17 (2004) 926 – 930

[77] J.L. Wang, R. Zeng, J.J. Kim, L. Lu and S.X. Dou, Effects of C substitution on the pinning mechanism of MgB_2, Phys. Rev. B 77 (2008) 174501

[78] S.R. Ghorbani, M. Darini, X.L. Wang, M.S.A. Hossain and S.X. Dou, Vortex flux pinning mechanism and enhancement of in-field j_c in succinic acid doped MgB_2, Sol. State Commum. 168 (2013) 1 - 5

[79] C.D. Wang, D.L. Wang, X.P. Zhang, C. Yao, C.L. Wang and Y.W. Ma, Aniline doping and high energy milling to greatly enhance electromagnetic properties of magnesium diboride superconductors, Physica C 489 (2013) 36 – 39

[80] C. Laliena, E. Matínez, L. A. Angurel and R. Navarro, Effect of ball milling and fatty acid addition on the properties of MgB_2 wires, IEEE Trans. Appl. Supercond. 25 (2015) 6200204

[81] D.N. Rakov, A.E. Vorobieva, P.V. Konovalov, E.V. Kotova, Yu.N. Belotelova and M.V. Polikarpova, Influence of carbon doping on MgB_2 superconducting properties, Physics Proc. 36 (2012) 1480 – 1485

[82] B. Savaşkan, E. Taylan Koparan, S.B. Güner, Ş. Çelik, K. Öztürk and E. Yanmaz, Effect of $C_4H_6O_5$ additions on the critical current density and lateral levitation force of bulk MgB_2, J. Low Temp. Phys. 181 (2015) 38 - 48

[83] Y.Z. Chua, H.T. Do, C. Schick, D. Zaitsau and C. Held, New experimental melting properties as access for predicting amino-acid solubility, RSC Adv. 8 (2018) 6365 – 6372

[84] A. Schaberg, R. Wroblowski and R. Goertz, Comparative study of the thermal decomposition behavior of different amino acids and peptides, J. Phys. Conf. Ser. 1107 (2018) 032013

[85] J. Li, Z. Wang, X. Yang, L. Hu, Y. Liu and C. Wang, Evaluate the pyrolysis pathway of glycine and glycylglycine by TG-FTIR, J. Anal. Appl. Pyrolysis 80 (2007) 247 – 253

[86] F. Cataldo, P. Ragni, S. Iglesias-Groth and A. Manchado, A detailed analysis of the properties of radiolized proteinaceous amino acids, J. Radioanal Nucl. Chem. 287 (2011) 287 – 911

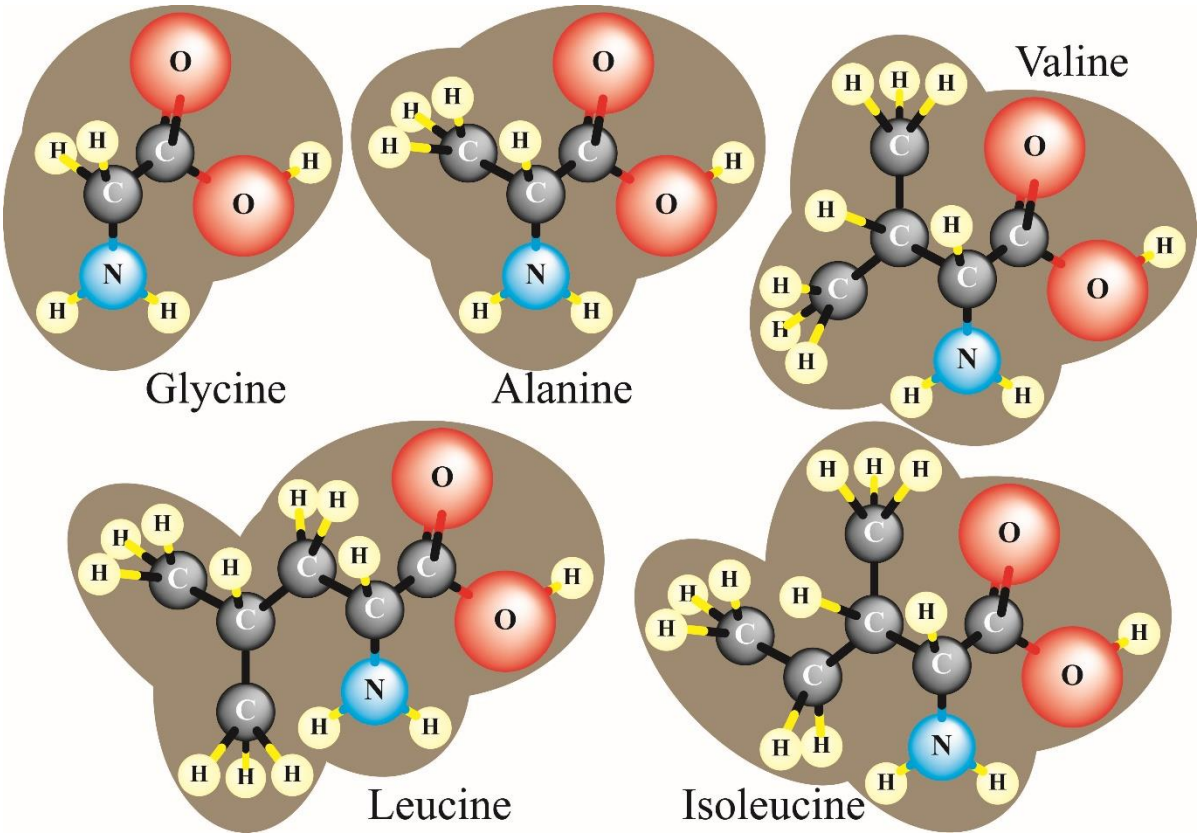

Figure 1

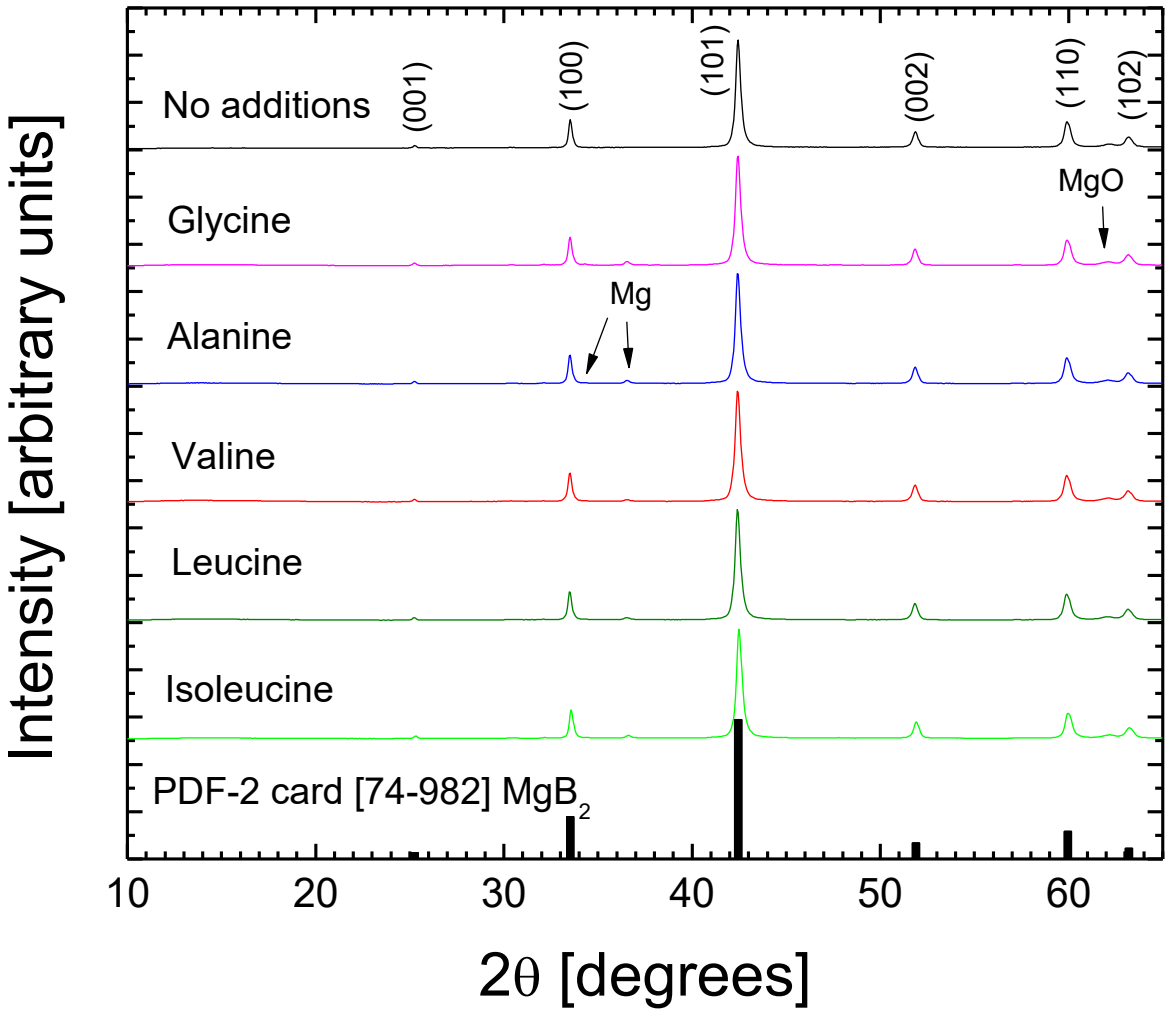
No additions
Glycine
Alanine
Valine
Leucine
Isoleucine
PDF-2 card [74-982] MgB2
(001)
(100)
(101)
(002)
(110)
(102)
MgO
Mg
Intensity [arbitrary units]
10
20
30
40
50
60
2θ [degrees]

Figure 2

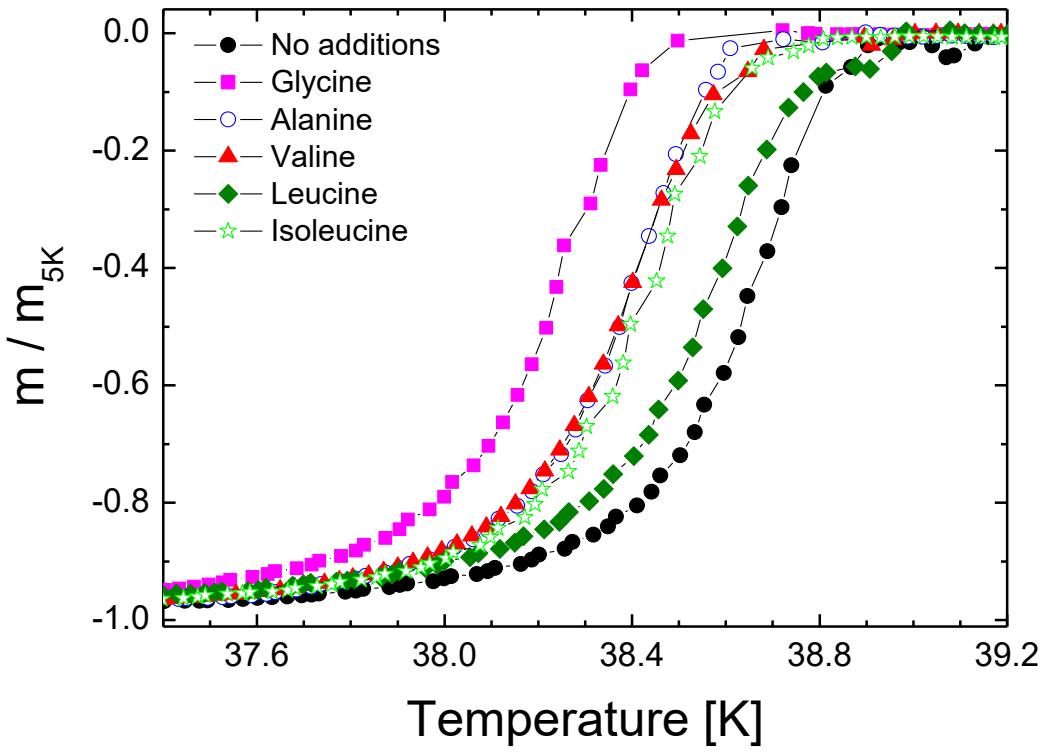
No additions
Glycine
Alanine
Valine
Leucine
Isoleucine
m / m5K
0.0
-0.2
-0.4
-0.6
-0.8
-1.0
37.6
38.0
38.4
38.8
39.2
Temperature [K]

Figure 3

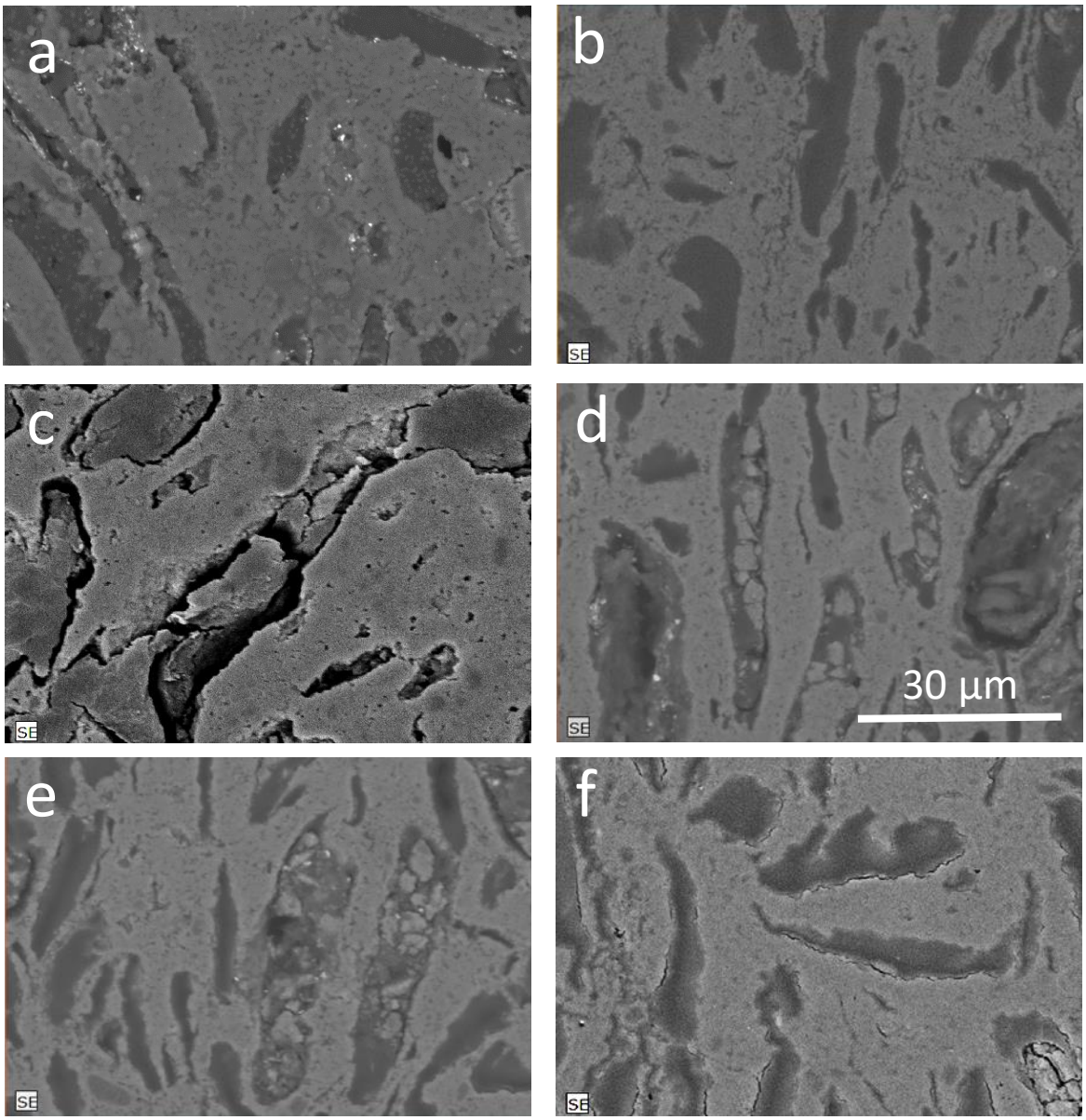

Figure 4

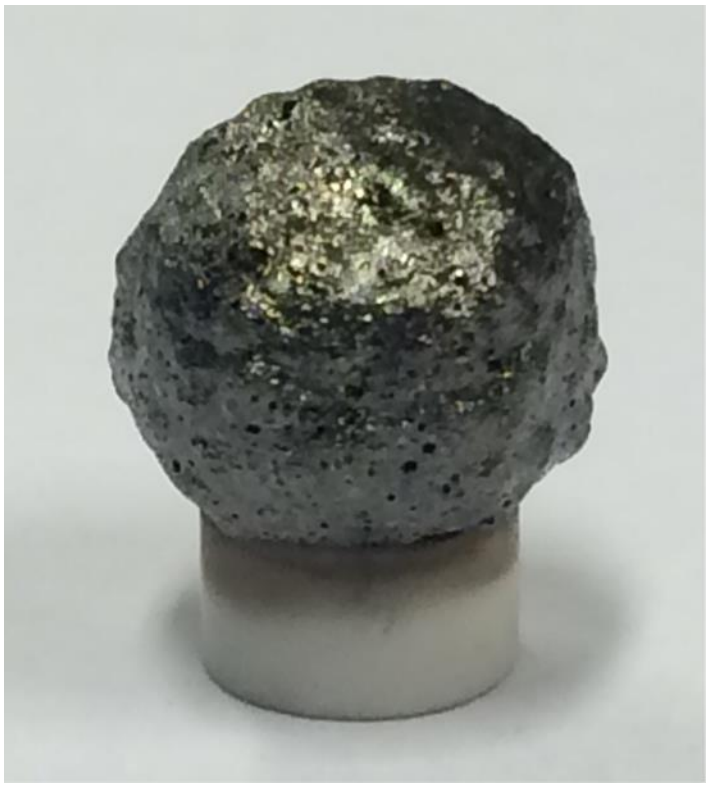

Figure 5

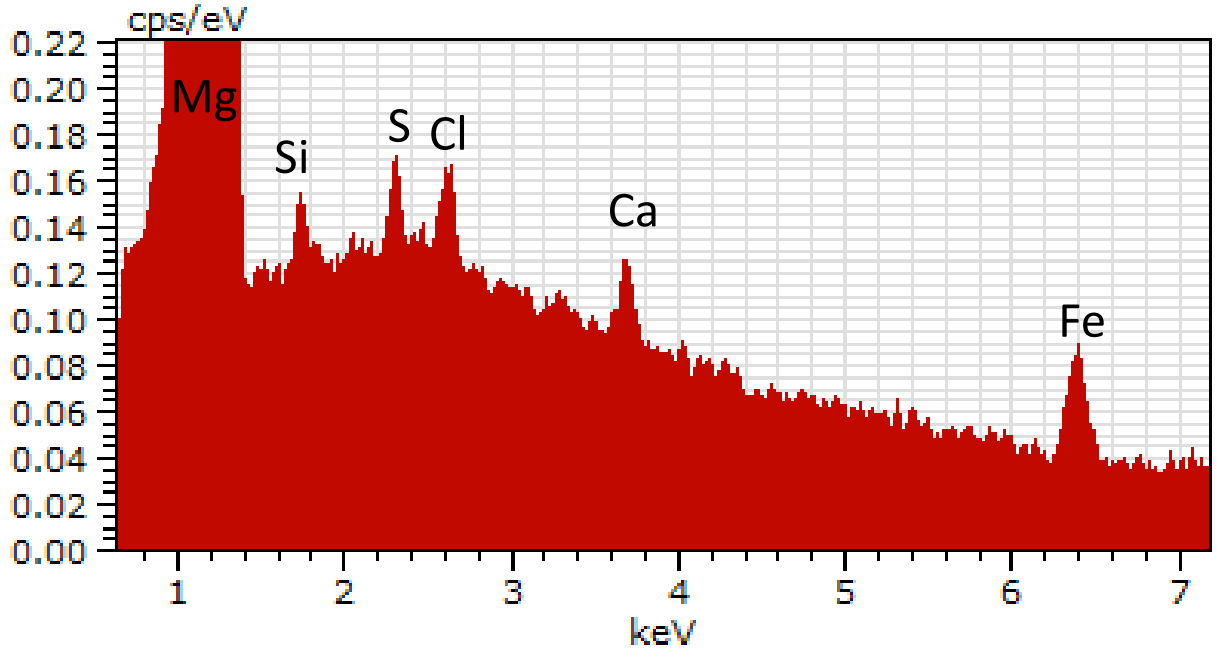

Figure 6

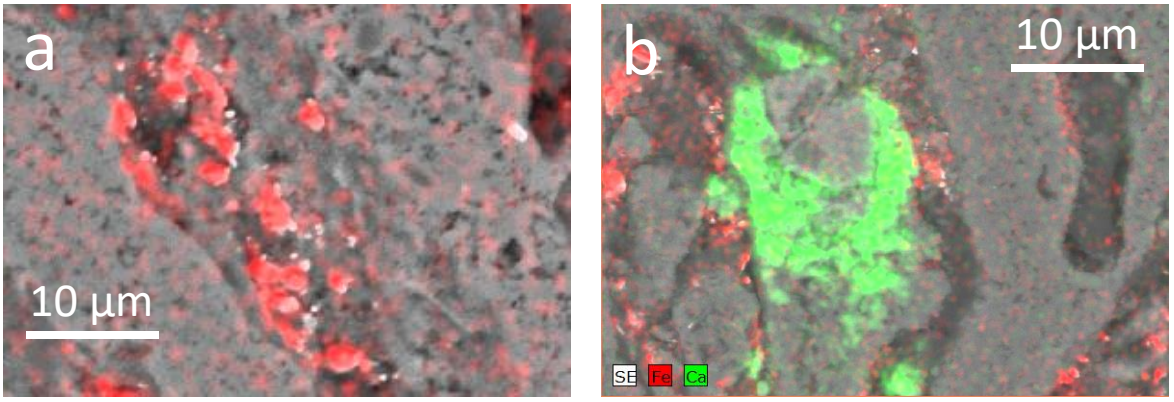

Figure 7

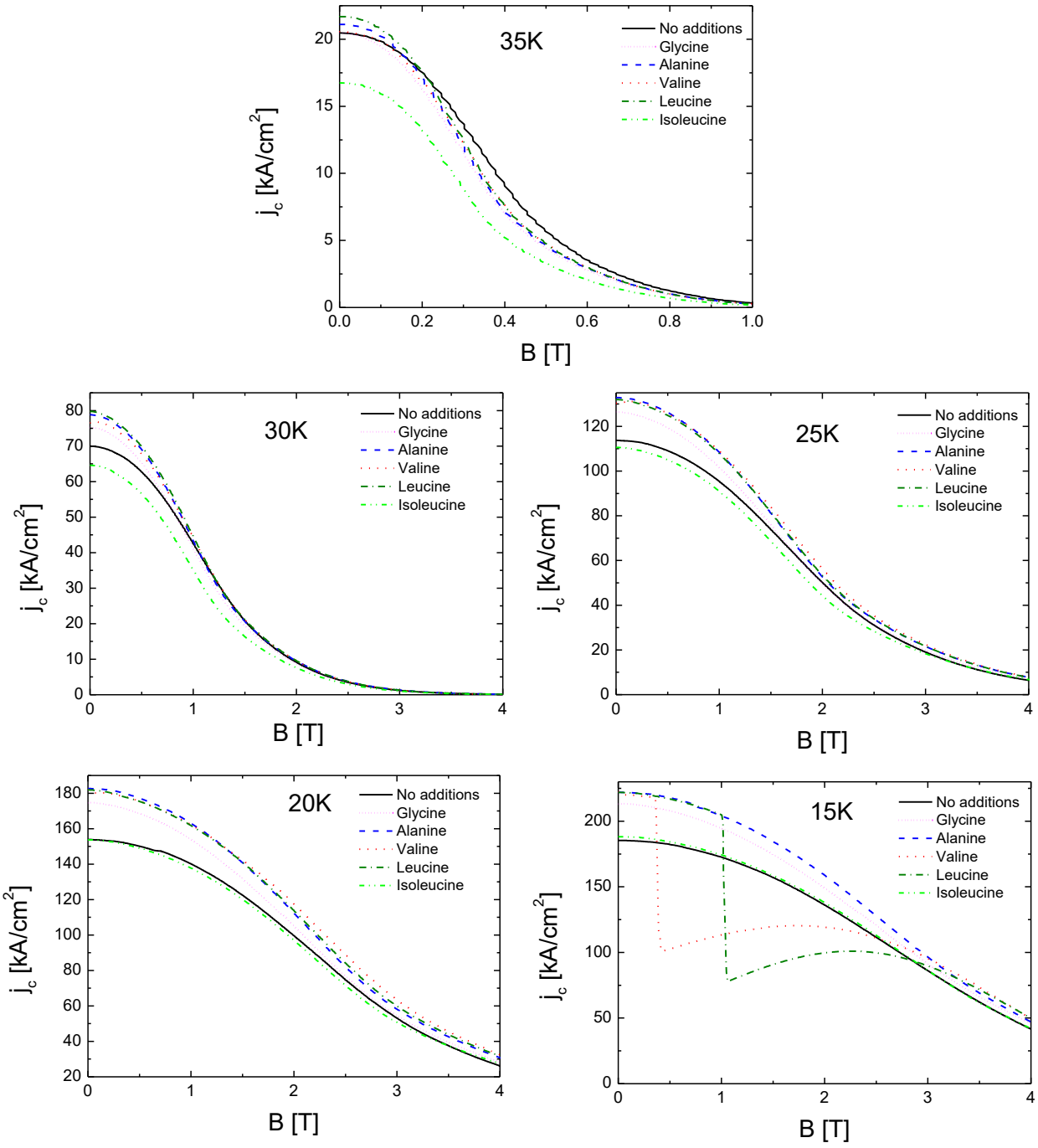
35K
30K
25K
20K
15K
No additions
Glycine
Alanine
Valine
Leucine
Isoleucine
j_c [kA/cm^2]
B [T]

Figure 8

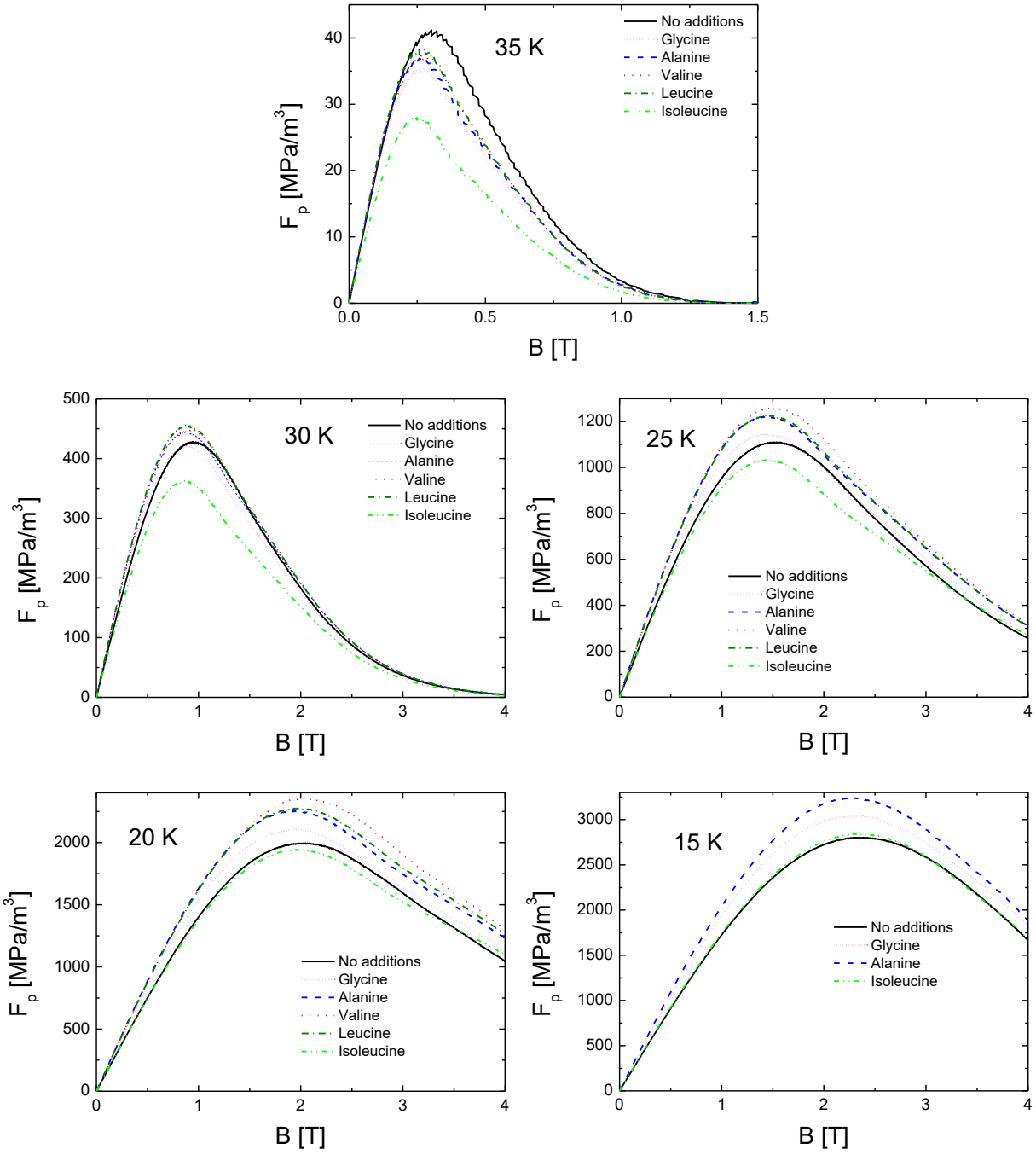
35 K
30 K
25 K
20 K
15 K
No additions
Glycine
Alanine
Valine
Leucine
Isoleucine
F_p [MPa/m^3]
B [T]

Figure 9

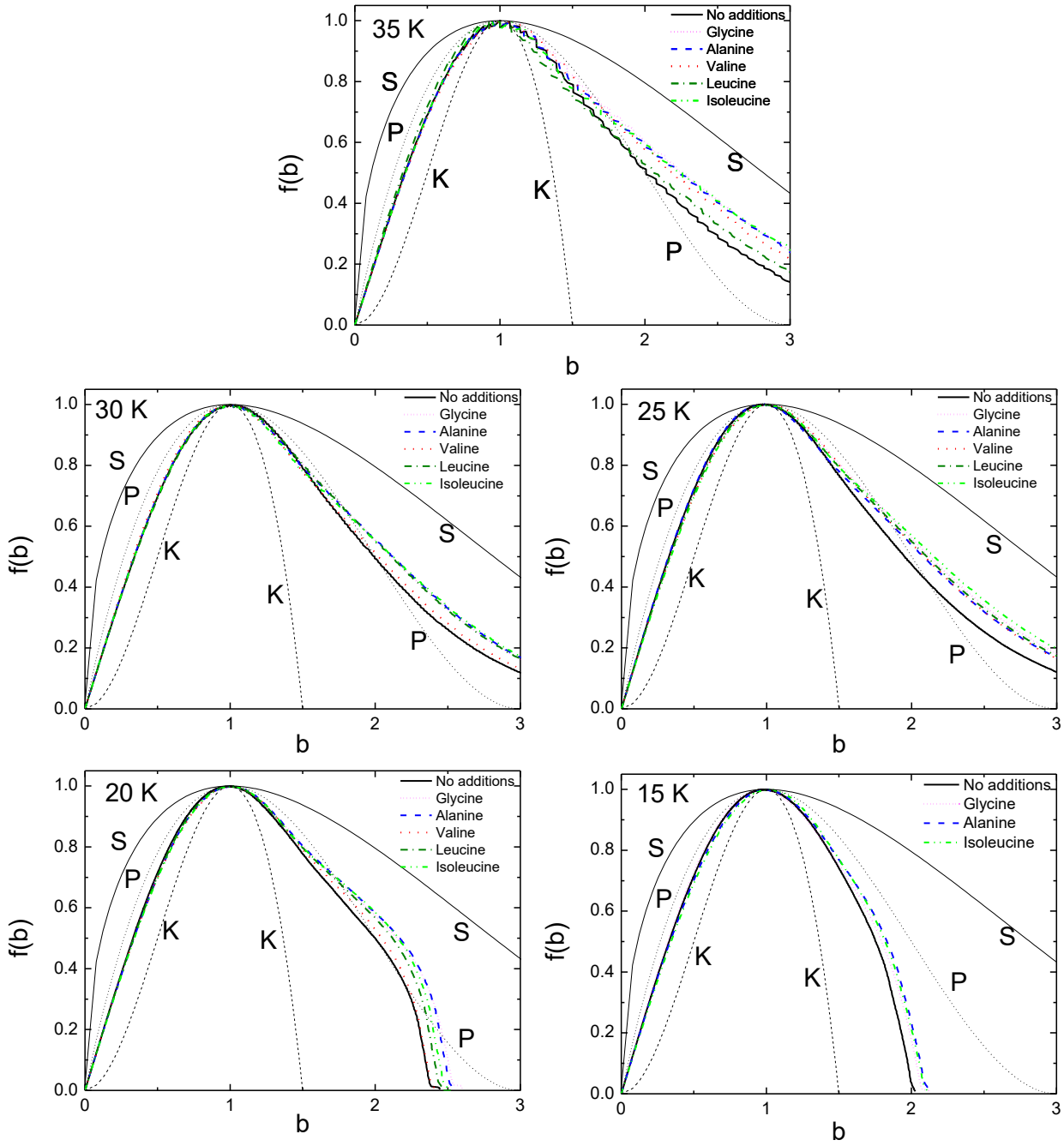
35 K
30 K
25 K
20 K
15 K
No additions
Glycine
Alanine
Valine
Leucine
Isoleucine
S
P
K
f(b)
b

Figure 10

Amino acid	Formula	wt.% C	Melting/Decomposition temperature [°C]
Glycine	$C_2H_5NO_2$	32.0	296 [83] / ≈225 [84] / ≈250 [65] / ≈280 [85] / ≈250 [68]
Alanine	$C_3H_7NO_2$	40.4	293.5 [86] / 335 [83] / 217-358 [68]
Valine	$C_5H_{11}NO_2$	51.3	298.1 [86] / 161-323 [68]
Leucine	$C_6H_{13}NO_2$	54.9	309.6 [86] / 207-342 [68]
Isoleucine	$C_6H_{13}NO_2$	54.9	294.5 [86] / 201-331 [68]

Table 1

Additive	a [Å]	c [Å]	T_c [K]	ΔT_c [K]	$FWHM_{(002)}$ [°] (2θ)	$FWHM_{(110)}$ [°] (2θ)	C_{XRD}	C_{Tc}	C_{nom} [Expressed as x in $MgB_{2-x}C_x$]
None	3.0849(2)	3.5219(3)	38.84(5)	0.63(9)	0.313(4)	0.363(6)	0.000	0.000	0.000
Glycine	3.0832(3)	3.5217(3)	38.37(5)	0.67(9)	0.316(4)	0.376(7)	0.008(3)	0.005(2)	0.006
Alanine	3.0839(3)	3.5227(3)	38.55(5)	0.60(9)	0.317(4)	0.375(8)	0.005(3)	0.004(1)	0.008
Valine	3.0837(3)	3.5219(3)	38.54(5)	0.65(9)	0.328(4)	0.387(8)	0.006(3)	0.004(1)	0.010
Leucine	3.0838(3)	3.5224(3)	38.73(5)	0.76(9)	0.320(4)	0.381(8)	0.005(3)	0.002(1)	0.011
Isoleucine	3.0844(3)	3.5227(3)	38.59(5)	0.63(0)	0.321(4)	0.385(8)	0.002(3)	0.003(1)	0.011

Table 2